RESEARCH ARTICLE-MECHANICAL ENGINEERING

Experimental Investigation and Modeling of Friction Coefficient and Material Removal During Optical Glass Polishing

Raj Kumar Pal[1] · Manoj Kumar[1] · Vinod Karar[1]

Abstract

Chemical mechanical polishing is a hybrid polishing technique having different applications in the semiconductor industry, biomedical and optical instrumentation, and defense equipment. The control and accuracy highly depend on the operator's skill due to limited knowledge of material removal behavior. This article attempts to fill this gap through an experimental investigation of friction coefficient and material removal rate as functions of abrasive particle size, normal load, relative velocity, and polishing time during BK7 optical glass polishing. In this article, Taguchi L18 mixed levels full factorial design was used to perform the experiments. Also, a temporal model for material removal rate is developed to study and investigate the mechanism of material removal. The results show the load per particle varies between 0.18×10^{-6} and 4.1×10^{-6} N, which led to the conclusion that material, are removed plastically from the workpiece surface and mechanical actions are dominant over chemical actions in material removal. The values of friction coefficient ($\mu \sim 0.1$) and 3D profilometer images also support this statement. The errors between predicted and experimental results are well within 8% and 12% for friction coefficient and material removal rate, respectively. This study is an important step toward the deterministic optical polishing process, leading to better control of material removal during the polishing of precision optical components.

Keywords Abrasive · Friction · Glass · Interface · Measurement · Modeling · Optical · Polishing · Surface · Tribology · Wear

Abbreviations

μ	Friction coefficient
k	Preston's constant
ρ	Density
a	Abrasive size
L	Polishing load
p	Polishing pressure
v	Speed (relative, polishing)
r	Offset distance between workpiece and polisher centers
s	Polisher speed
w	Weight
D	Diameter of the workpiece
A_r	Workpiece to polisher area ratio
Ns	Number of abrasive particles bearing the polishing load
t_p	Pad thickness
F_a	Load per particle
V_a	Volume of abrasive particle
$x, y, z, \gamma, \alpha, \beta, \varepsilon$	Fitting parameters
MRR	Material removal rate
CMP	Chemical mechanical polishing
OA	Orthogonal array
AFM	Atomic force microscope
ANOVA	Analysis of variance
Adj SS	Adjusted sum of square
Adj MS	Adjusted mean square
DOF	Degrees of freedom
SR	Surface roughness
CCI	Coherence correlation interferometry

✉ Raj Kumar Pal
  rajkpal@csio.res.in

1 Imaging, Avionics, and Display Systems (IADS),
  CSIR-Central Scientific Instruments Organisation
  (CSIR-CSIO), Sector-30, Chandigarh 160030, India

1 Introduction

Optical fabrication generally involves the fabrication of precision components made from glass material. Glass, apart from being optically transparent, is highly brittle. Hence, the machining of glass poses practical challenges [1–4]. It becomes highly important to understand the material removal behavior of the machining process to achieve the desired surface and shape characteristics [5–7]. The optical polishing process generally involves the rubbing of workpiece and polisher surfaces in the presence of cerium oxide-based slurry [8]. The material removal behavior of the optical polishing process determines the characteristics of the surface achieved after polishing [9–11]. Material removal during the polishing process involves mechanical abrading forces and chemical actions taking place at the polishing interface [12–15]. However, the actual scenario at the interface is determined by the process parameters of the polishing process. The value of the friction coefficient at the workpiece-polisher interface is an indicator of whether the contact between the workpiece and polisher is of solid–solid contact mode ($\mu \sim 0.1$), hydroplaning mode ($\mu \sim 0.001$ to 0.01), or mixed-mode type ($\mu \sim 0.01$ to 0.1) [16–18]. Frictional characteristics of the workpiece-polisher interface generally depend upon normal load, relative velocity, slurry characteristics, polishing time, etc. [19–22]. However, they are not explicitly defined scientifically for the optical glass polishing process.

Yu et al. [23] explored the nanoscale friction during the interaction of single-particle CeO_2 and BK7 glass surfaces and observed that it is the interfacial friction that is responsible for material removal during the polishing process. The chemical phenomenon (hydrolysis of Si–O–Si bond) occurs very little due to the chemical inertness of BK7 optical glass. However, depending on the chemical affinity of the substrate, the mechanism of material removal may vary. Promising results have been reported by Suratwala et al. [24] wherein a Hertzian contact mechanics-based optical polishing model has been proposed. Slurry particle size distribution has been reported to play a significant role in defining the material removal rate and mechanism.

Normal load when applied over the workpiece gets distributed over the abrasive particles which then get embedded into the workpiece surface and remove material due to the relative motion [25]. Hence, the amount and mechanism of material removal depend upon the load transferred to each particle. Suratwala et al. [26] reported that if the load per particle is higher than 5×10^{-5} N and lower than 0.1 N for a fused silica glass workpiece, material removal would take place through a plastic removal mechanism; when it is quite low, below 5×10^{-5} N, chemical actions become dominant in material removal. Hence, load per particle is another indicator of the material removal mechanism; however, it is not sufficient.

The CMP process capabilities can be enhanced through some additives that chemically activate the polishing surface [27, 28]. The chemical effect has been increased by 133% through a chemical reaction by adding citric acid. The material wear is dominated by plastic deformation and material removal occurs at the micro-nano level, i.e., at the size of the abrasive particle [29]. Luo et al. conducted the polishing studies at different pH slurries and reported that Preston's equation needed modification to present the data better. The authors have included two additional factors include chemical reactivity and polish rate (velocity term) in Preston's equation [30]. Murthy et al. study the mechanical aspect of the CMP process by evaluating the Von Mises stress on the workpiece. The result shows the radial deformation of the polisher and carrier film under the action of downforce [31].

CMP is an important process for manufacturing the IC circuit, a key component in the semiconductor industry. Lee et al. discussed the environmental issues related to the CMP process due to the enormous demands of the semiconductor industry. From a sustainability point of view, various techniques were purposed and discussed for post-processing related to wastewater, CMP slurry, and other consumables [32]. Further, Seo reviewed the critical issue related to safety and toxicity issues related to the CMP process. The undesirable toxic gases such as phosphine and arsine during the polishing of III-V materials [33]. Terell et al. reviewed the hydrodynamic studies related to the CMP process, as slurry behavior across the lap-workpiece interface defines the wear distribution. The authors reported that no complete study is available that explains and predicts slurry behavior. The oversimplified and unrealistic assumption made in model development needs re-investigation [34].

In this study, BK7 optical glass is used as the workpiece material for performing the experiments. It is generally used for various applications in the basic research, industrial, defense, and medical sector which require high precision surfaces with minimum surface and subsurface defects [9, 35–37]. Some of the specific applications are beam combiners and folding mirrors for head-up displays, glass mirrors for the astronomical telescope, electronic substrates, mirrors and polarizers for lasers, a substrate for biological sample analysis, etc. [9, 38–41]. Polishing such a substrate, which is hard as well as brittle, is critical and time-consuming [42]. In this study, the frictional force at the polishing interface is measured and the friction coefficient is modeled as a function of abrasive particle size, normal load, and relative velocity. Finally, an empirical model, for material removal during the polishing process, is proposed as a function of friction coefficient, normal load, and relative velocity. Authors have also attempted to model the load per particle to describe the mechanism of material removal during polishing of BK7 optical glass, also supported by values of friction coefficient.
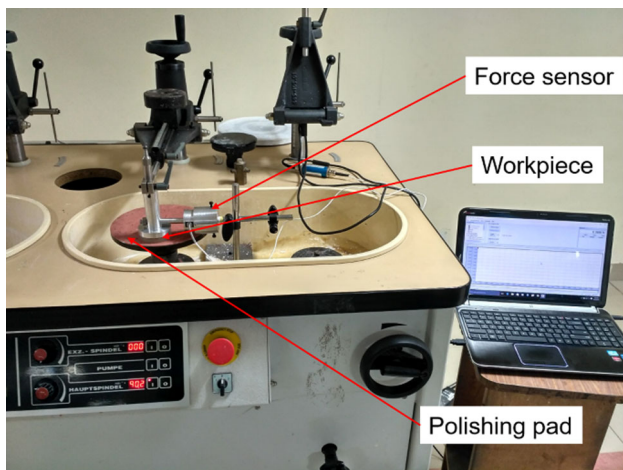
Fig. 1 Experimental setup showing the interfacing of load cell with the full aperture optical polishing machine

Table 1 Levels and values of control parameters

Parameters	Levels		
Abrasive size (μm): a	1.4		3.2
Normal load (N): L	10	14	18
Relative velocity (m/s): v	0.352	0.528	0.704

Table 2 L18 parameters summary table

Run	Abrasive size	Normal load	Relative velocity
1	1	1	1
2	1	1	2
3	1	1	3
4	1	2	1
5	1	2	2
6	1	2	3
7	1	3	1
8	1	3	2
9	1	3	3
10	2	1	1
11	2	1	2
12	2	1	3
13	2	2	1
14	2	2	2
15	2	2	3
16	2	3	1
17	2	3	2
18	2	3	3

2 Materials and Methods

Frictional force during the polishing process is measured using a miniature load cell (Capacity 25 lbs, Make: Interface, USA). The experimental setup is shown in Fig. 1. The workpiece is kept at an offset from the center of the polisher to record the tangential force generated through the rubbing action of the rotating polisher. Schott BK7 optical glass is used as substrate (ø 55 mm, height 10 mm) for the experiments. In this study, Taguchi's L$_{18}$ orthogonal array is used to study the relationship between Friction coefficient and MRR with the polishing parameters, viz., abrasive size, normal load, and polisher speed, having different levels (Table 1). The values of parameters are selected based on initial random experiments. Table 2 presents Taguchi's standard L$_{18}$ orthogonal array.

Before polishing, the workpiece is lapped over the iron lap tool using two different grades of emery (mainly Al$_2$O$_3$) in the following order: 302 (M2) and 303 (M3) having mean particle sizes of 28 μm and 14.5 μm, respectively, to make the workpieces ready for polishing. The sample weight is measured using a weighing balance (Wensar MAB 220, max. capacity 220 g, resolution of 0.1 mg) before polishing. Then the sample is blocked on a custom-designed aluminum blocking tool. The abrasive slurry of fixed concentration (8.25% by weight, based on our earlier study [9]) is prepared by mixing 8.25 g of cerium oxide (CeO$_2$) powder (Unicer 657 and Rhodite 200, physical properties are listed in Table 3, supplier Universal Photonics Inc., US) with 100 ml of deionized water.

Polyurethane pad (LP-66, supplier Universal Photonics Inc., US) is used as polisher material. To minimize the effect of pad elastic properties on frictional characteristics, a minimum thickness of 0.5 mm is taken [19]. The physical properties of the polishing pad are shown in Table 4 [43]. Abrasive slurry is fed manually at constant intervals of time. Because of the polisher rotation, the tangential force exerted on the workpiece surface gets transferred to the sensor via a connecting rod and is recorded. Frictional force data are recorded at a frequency of 100 Hz. Before starting the data acquisition, it has been ensured that the workpiece is in proper contact with the polishing pad surface. Each polishing experiment is run for 10 min at room temperature (22 °C). The frictional force vs time data for 18 different combinations of parameters (see Table 2) are recorded by the force sensor. The surface texture of the workpiece sample is observed through Taylor Hobson CCI Optics before and after polishing. Measurements are taken using a 20X objective lens. After polishing, sample weight is again measured using a precision weighing balance.

Table 3 Physical properties of abrasive particles

S/N	Abrasive type	Base material	Appearance	Particle size (µm)
1	Unicer 657	Cerium Oxide	White powder	Range: 1.0–1.75 Mean: 1.375
2	Rhodite 200	Cerium Oxide	Orange-brown powder	Range: 2.6–3.8 Mean: 3.2

Table 4 Properties of polishing pad

Pad type	Filler material	Thickness (mm)	Shore hardness (A)	Density (g/cc)
LP-66	Cerium Oxide	0.5	78	0.42
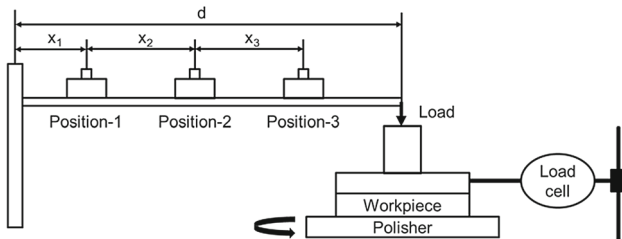
Fig. 2 Schematic of normal load application during the polishing process

3 Modeling and Calculations

3.1 Normal Load

The schematic of the application of normal load during the optical polishing process is shown in Fig. 2. Load-1 (L_1), Load-2 (L_2), and Load-3 (L_3) correspond to two different positions of weight 'w' and may be calculated as:

Normal load when weight 'w' at position-1:

$$L_1 = \left(\frac{x_1}{d}\right)w \tag{1}$$

Normal load when weight 'w' at position-2:

$$L_2 = \left(\frac{x_1 + x_2}{d}\right)w \tag{2}$$

Normal load when weight 'w' at position-3:

$$L_3 = \left(\frac{x_1 + x_2 + x_3}{d}\right)w \tag{3}$$

Here $x_1 = 165$ mm, $x_2 = 80$ mm, $x_3 = 80$ mm, $d = 433$ mm, and $w = 2.5$ kg. Hence values of L_1, L_2 and L_3 are computed to be approximately 10 N, 14 N and 18 N, respectively.

3.2 Relative Velocity

Relative velocity v *(mm/min)* is calculated as:

$$v = \frac{2\pi s r}{60000} \tag{4}$$

where s is polisher speed (rpm), and r is the offset distance between the workpiece and polisher centers (56 mm).

3.3 Friction Coefficient

Friction coefficient (μ) is calculated as below:

$$\mu = \frac{F}{L} \tag{5}$$

where F is measured friction force, and L is normal load (from Eqs. 1, 2, and 3).

3.4 Material Removal Rate

Material Removal Rate, MRR (nm/sec) is calculated using the weight difference method [9]:

$$MRR = \frac{4 \times \Delta m \times 10^9}{\Delta t \times \rho \times \pi \times D^2} \tag{6}$$

where Δm is the change in mass of the workpiece in grams, Δt is the polishing time (seconds), ρ is the density of the BK7 glass workpiece (2.51 g/cm^3), and D is the diameter of the workpiece in mm.

3.5 Load per Particle

Modeling of load applied per particle has been carried out considering some assumptions based on observations and prior knowledge. First of all, it is assumed that all the abrasive particles are spherical with an average diameter of 'a'. Hence, the volume of a single abrasive particle, V_a(cm^3) is defined as:

$$V_a = \left(\frac{4}{3}\pi\left(\frac{a}{2}\right)^3\right)10^{-12} \tag{7}$$

where a is abrasive particle size (in µm), and the mass of one abrasive particle, m_a(grams) is then defined as:

$$m_a = V_a d_a \tag{8}$$

where d_a is the density of abrasive particles in grams per cubic centimeters (g/cm^3).

Let x grams of abrasive powder be added to 100 ml of deionized water to prepare a slurry of $x\%$ (by weight) concentration. For the present study, the slurry concentration is 8.25% (by weight). Hence, several abrasive particles in x grams of abrasives are:

$$N_a = \frac{x}{m_a} \tag{9}$$

Abrasive slurry is supplied at the rate of 0.1 ml/min. Hence the number of particles added every minute is:

$$N_0 = \frac{0.1 \times N_a}{\left(100 + \frac{x}{d_a}\right)} \tag{10}$$

Thus, the total number of abrasive particles present on the polisher surface at any moment is given by:

$$N(t) = N_0 + dt \tag{11}$$

where t is time in minutes and has values from integer 0 to 9 and N_0 is the number of abrasive particles at $t = 0$. d is a parameter that gives the net amount of slurry being added at the interface after every one minute, as some of the slurries get flow away due to centrifugal force (a function of polisher speed), and its values are observed for the three different polisher speeds, i.e., 60 rpm, 90 rpm, and 120 rpm, are $0.6N_0$, $0.55N_0$, and $0.5N_0$, respectively.

The workpiece to polisher area ratio, A_r:

$$A_r = \frac{D_w^{\,2}}{D_p^{\,2}} \tag{12}$$

where D_w and D_p are diameters of the workpiece and polisher. Hence, several abrasive particles under the workpiece surface at a point in time are:

$$N_{aw} = A_r N(t) \tag{13}$$

It is observed that some of the slurries get settled into the pores of the polishing pad, hence do not bear the polishing load. The area of the open pores is approximately 1.5% of the total polishing pad area. Hence, the number of particles lying in the open pores under the contact area is:

$$N_p = \frac{0.015 \pi D_w^{\,2} t_p N_a}{4\left(100 + \frac{x}{d_a}\right)} \tag{14}$$

where t_p is the pad thickness. Hence, the number of active particles bearing the polishing load is:

$$N_s = N_{aw} - N_p \tag{15}$$

Assuming that the normal load is uniformly distributed across the workpiece-polisher interface, the load per particle may be calculated as:

$$F_a = \frac{L}{N_s} \tag{16}$$

where L is the normal load in newton (N).

4 Results and Discussion

The frictional force vs. time data recorded by the force sensor is analyzed and the friction coefficient is calculated based upon that. The frictional force data are recorded for 10 min of polishing, however, to avoid the initial sudden variations in frictional force, the average value of the last 6 min of data is considered for computation. The obtained experimental results comprising friction force, friction coefficient, and MRR are listed in Table 5.

4.1 Friction Coefficient Model

The main and interaction effects plots for friction coefficient are shown in Fig. 3. It is observed that the friction coefficient increased approx. 43% when abrasive size is increased from 1.375 µm to 3.2 µm which is because of greater resistance faced by larger size particles at the workpiece-polisher interface. Increasing the normal load deepens the penetration of abrasive particles into the workpiece surface and also increases the effective area of contact between the abrasive particle and workpiece surface [44, 45], leading to increased resistance which results in increased frictional force. But the variation in friction coefficient is not quite significant, only an increase of approx. 5% in friction coefficient with the change of normal load from 10 to 14 N and also from 14 to 18 N. However, friction coefficient exhibits inverse behavior with polishing speed. But it is observed to decrease with an increase in relative velocity. Friction coefficient decreased approx. 35% with increase in relative velocity from 0.352 m/s to 0.528 m/s and also from 0.528 m/s to 0.704 m/s. It may be the result of aquaplaning effect, i.e., formation of liquid film at the interface at high relative velocity [20]. Moreover, the adhesion component of the friction coefficient dominates over the deformation component at a higher relative velocity which leads to a reduction in the friction coefficient [20, 46]. The results are in agreement with those reported in earlier researches [19, 20, 22]. Based on the observations, it may be stated that:

$$\mu \propto a \tag{17}$$

$$\mu \propto L^\beta \tag{18}$$

Table 5 Experimental and modeling results

| Run	Results based on experimental data							Results based on modeling of load per particle			
	Abrasive size (μm): a	Normal load (N): L	Relative velocity (m/s): v	Frictional force (N): F	Friction coefficient: μ	MRR (nm/s)	Preston's constant (m²/N): k_R	Avg. no. of active abrasive particles: N_s	Avg. load per particle (N): F_a	Work done/area/time (Nm⁻¹ s⁻¹): W	Preston's constant (m²/N): k
1	1.375	10	0.352	2.09	0.209	0.20	3.2079E−13	5.6904E+07	1.80E−07	3.60	1.3216E−13
2	1.375	10	0.528	1.39	0.139	0.36	2.7216E−13	5.4554E+07	1.86E−07	5.36	1.5953E−13
3	1.375	10	0.704	0.78	0.078	0.48	2.1632E−13	5.3153E+07	1.90E−07	7.12	1.6005E−13
4	1.375	14	0.352	3.00	0.214	0.58	3.2394E−13	5.6904E+07	2.51E−07	5.03	2.7376E−13
5	1.375	14	0.528	2.28	0.163	0.79	2.9028E−13	5.4554E+07	2.61E−07	7.50	2.5006E−13
6	1.375	14	0.704	1.23	0.088	0.68	2.2660E−13	5.3153E+07	2.67E−07	9.98	1.6196E−13
7	1.375	18	0.352	4.04	0.225	1.04	3.3017E−13	5.6904E+07	3.23E−07	6.47	3.8179E−13
8	1.375	18	0.528	3.08	0.171	1.17	2.9611E−13	5.4554E+07	3.35E−07	9.65	2.8805E−13
9	1.375	18	0.704	1.75	0.097	1.32	2.3644E−13	5.3153E+07	3.43E−07	12.82	2.4453E−13
10	3.200	10	0.352	2.87	0.287	0.45	3.6425E−13	4.7652E+06	2.14E−06	3.60	2.9736E−13
11	3.200	10	0.528	1.96	0.196	0.64	3.1276E−13	4.5683E+06	2.22E−06	5.36	2.8362E−13
12	3.200	10	0.704	1.21	0.121	0.81	2.5773E−13	4.4510E+06	2.27E−06	7.12	2.7009E−13
13	3.200	14	0.352	4.27	0.305	0.56	3.7306E−13	4.7652E+06	3.00E−06	5.03	2.6432E−13
14	3.200	14	0.528	2.91	0.208	0.87	3.1987E−13	4.5683E+06	3.11E−06	7.51	2.7539E−13
15	3.200	14	0.704	1.75	0.125	1.17	2.6131E−13	4.4510E+06	3.18E−06	9.98	2.7867E−13
16	3.200	18	0.352	5.56	0.309	1.00	3.7514E−13	4.7652E+06	3.86E−06	6.47	3.6710E−13
17	3.200	18	0.528	3.97	0.220	1.40	3.2772E−13	4.5683E+06	4.00E−06	9.65	3.4467E−13
18	3.200	18	0.704	2.42	0.135	1.82	2.6910E−13	4.4510E+06	4.09E−06	12.82	3.3715E−13
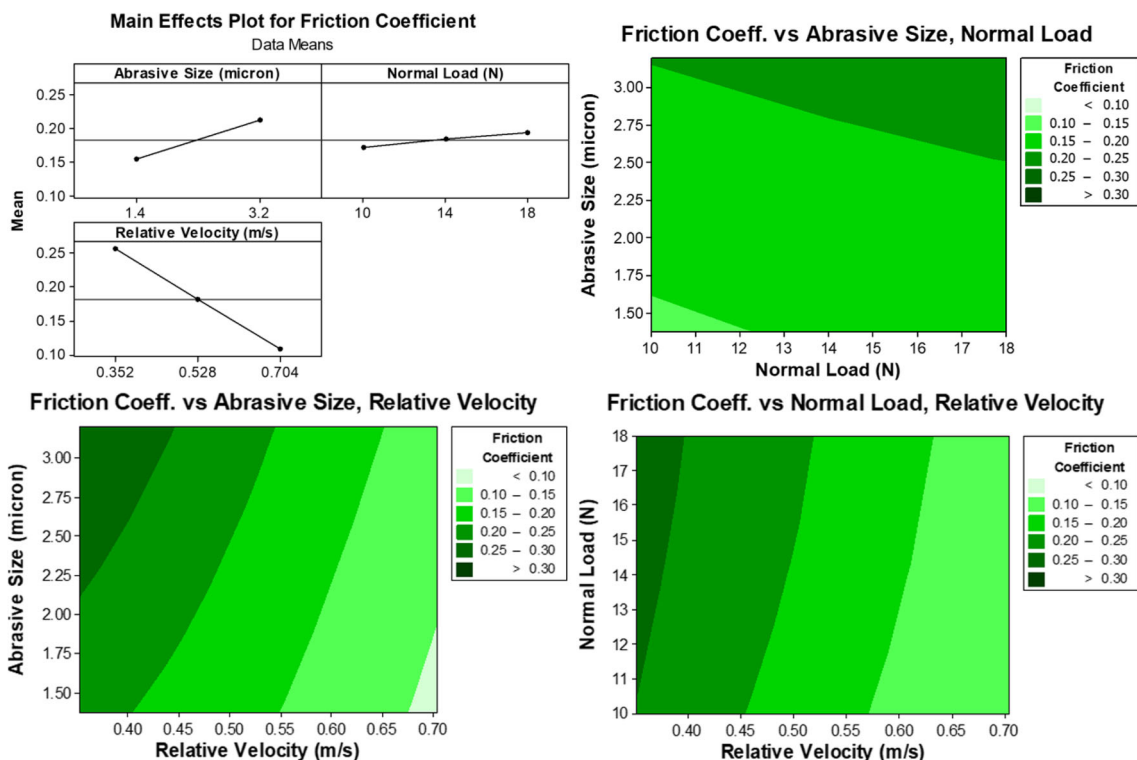
Fig. 3 Main effects and interaction plot for friction coefficient

$$\mu \propto \frac{1}{v^\varepsilon} \tag{19}$$

Hence, by combining the above equations, we get:

$$\mu \propto \frac{a^\alpha L^\beta}{v^\varepsilon} \tag{20}$$

Here, a: abrasive size; L: normal load; v: polishing speed; α,β,ε: fitting parameters.

The friction coefficient is then plotted against $(a^\alpha L^\beta)/v^\varepsilon$ and values of the fitting parameters are found through iterations using nonlinear regression analysis (*Algorithm: Gauss–Newton, Iterations: 200, Final Sum of Squares of Errors (SSE): 0.0003905*) while fitting the data in the sigmoidal curve, which better represents the coefficient of friction [19] (Fig. 4):

$$\mu = 1 - \frac{0.274}{1 - 2.2 e^{-\left(\frac{a^{1/3}L^{1/4}}{v}\right)^{0.112}}} \tag{21}$$

Here, μ is friction coefficient; a is abrasive size (microns); L is polishing load (N); v is relative velocity (m/s).

4.2 Material Removal Rate Model

The main and interaction effects plots for MRR are shown in Fig. 5. It is observed that MRR increases with an increase in
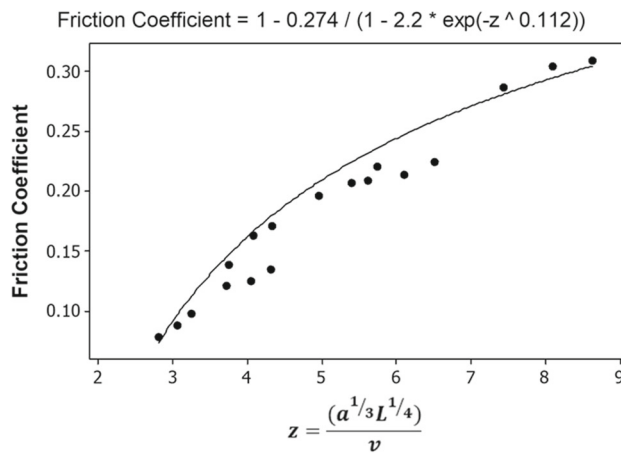

Fig. 4 An empirical formulation for friction coefficient

abrasive size, polishing load as well as polishing speed [10]. Increasing the abrasive size and polishing load increases the contact area (refer to Hertz contact equation [47]) between the abrasive and workpiece surface, hence leading to the removal of more material [23]. Based on these observations, the following relations are developed:

$$MRR \propto a^x \tag{22}$$
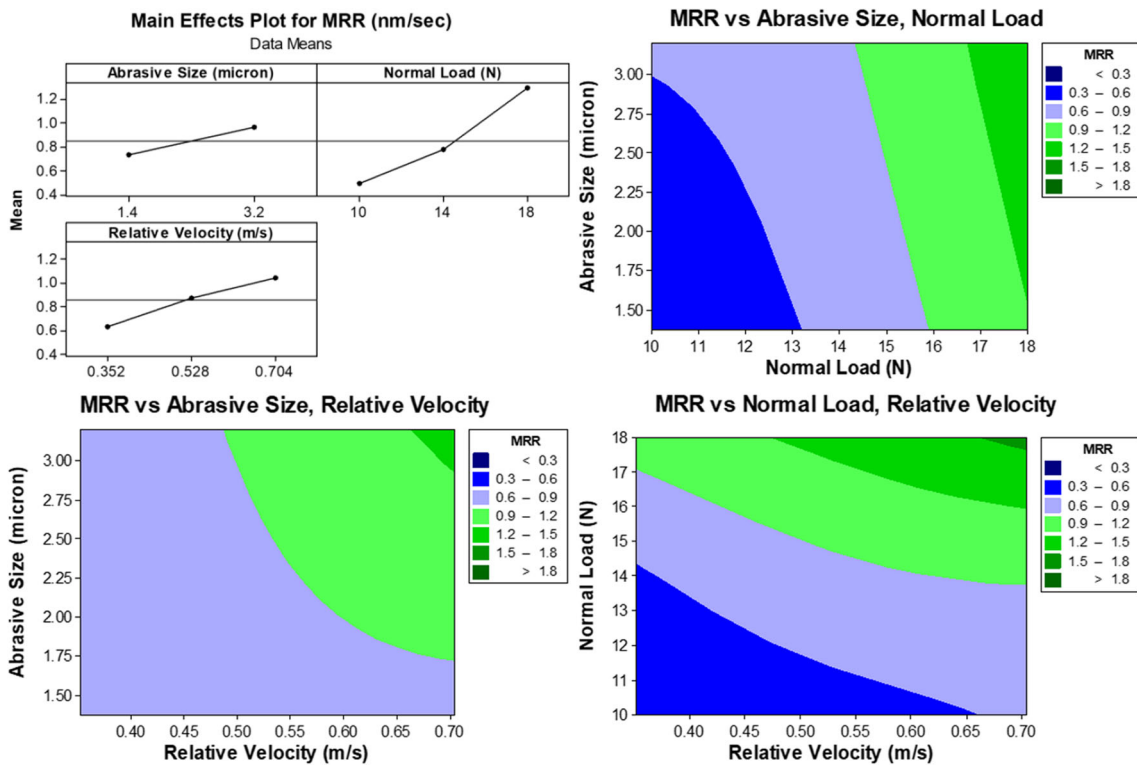
$$MRR \propto L^y \tag{23}$$

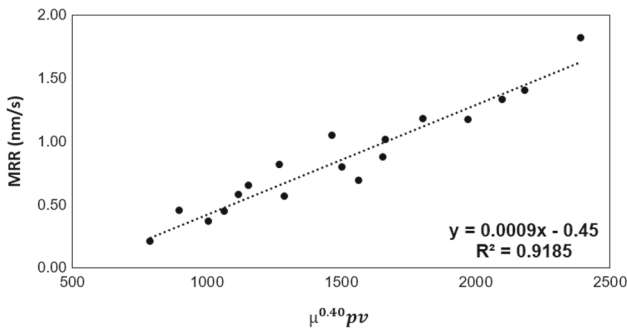**Fig. 5** Main effects and interaction plot for MRR

Fig. 6 An empirical formulation for MRR

$$MRR \propto v^z \tag{24}$$

And, as material removal is due to the work done by friction force:

$$MRR \propto \mu^\gamma \tag{25}$$

Hence, by combining the above equations, we get:

$$MRR \propto \mu^\gamma a^x L^y v^z \tag{26}$$

where a is abrasive size; L is polishing load; v is polishing speed; x, y, z, γ are fitting parameters.

MRR is then plotted against $\mu^\gamma a^x L^y v^z$ and values of the fitting parameters are found through iterations while fitting the data in a linear equation ($R^2 = 0.9185$) (Fig. 6):

$$MRR = c_1\left(\mu^\gamma pv\right) \tag{27}$$

Here, *MRR* is material removal rate (nm/sec); μ is friction coefficient; p is polishing pressure (N/m^2); v is relative velocity (m/s); γ is fitting parameter, c_1 is a constant. The values of c_1 and γ are 0.0006 and 0.4, respectively.

The equation may be re-written as:

$$MRR = k_R pv \tag{28}$$

where k_R is the new modified Preston's constant and is equal to $c_1\mu^\gamma$. The modified Preston's constant is a function of friction coefficient (μ), which itself is a function of abrasive size, normal load, and relative velocity, as mentioned in Eq. (21). Based on the experimental data, the value of k_R is observed to lie in the range of 2.1632×10^{-13} to 3.75145×10^{-13} m^2/N. Preston's constant with values of similar order ($\sim 10^{-13}$ m^2/N) has been reported by other researchers [12, 48].
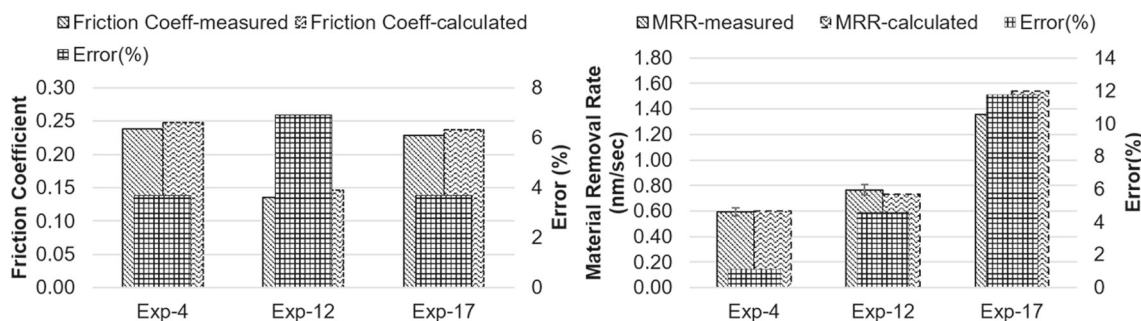
Fig. 7 Validation of empirical formulation for friction coefficient and MRR

4.3 Experimental Validation

To validate the empirical equations for friction coefficient and MRR, three experiments (Experiment #4, #12, and #17) were repeated. These experiments were chosen in such a way that all the variations of parameters are covered. Then, the measured data are plotted against the calculated data and is shown in Fig. 7 for friction coefficient and MRR. The error between measured and calculated values is within 8% for friction coefficient and 12% for MRR. Hence, the equations for friction coefficient and MRR are validated.

4.4 Analysis of Variance

The Analysis of Variance (ANOVA) is used to verify the significance of the effects of the process parameters on friction coefficient and MRR. ANOVA results corresponding to friction coefficient are shown in Table 6. The regression equation obtained for friction coefficient is:

$$\mu = 0.202749 + 0.071394a + 0.00345903L - 0.256612v$$
$$- 0.000171619aL - 0.0704038av - 0.000772886Lv$$

$$(29)$$

The P-value of the regression equation is zero which means that at least one of the coefficients of the regression equation is nonzero. ANOVA table displaying P values < 0.05 indicates that the particular parameters and their interactions are significant in defining the friction coefficient at the workpiece-polisher interface. And the F values (highest the most significant) indicate that the order of significance is abrasive size, the interaction of abrasive size and relative velocity, and relative velocity. $R^2 = 99.64\%$ indicates that the regression model explains 99.64% of the variation in the friction coefficient data. The adjusted R^2 is 99.94%. R^2 (pred) = 99.09% indicates that the model explains 99.09% of the variation in friction coefficient when the model is used for prediction.

ANOVA results corresponding to MRR are shown in Table 7. The regression equation obtained for MRR is:

$$MRR^{0.5} = -0.37421 + 0.0603051a + 0.0737677L$$
$$- 0.0377441v - 0.00873868aL$$
$$+ 0.259978av + 0.00496572Lv \qquad (30)$$

The P-value of the regression equation is zero which means that at least one of the coefficients of the regression equation is nonzero. ANOVA table displaying P values < 0.05 indicates that the particular parameters and their interactions are significant in defining the material removal rate during polishing of BK7 optical glass. And the F values (highest the most significant) indicate that the order of significance of the process parameters is normal load, the interaction of abrasive size and relative velocity, and the interaction of abrasive size and normal load. $R^2 = 97.22\%$ indicates that the regression model explains 97.22% of the variation in the MRR data. The adjusted R^2 is 95.70%. R^2 (pred) = 91.95% indicates that the model explains 91.95% of the variation in MRR when the model is used for prediction.

4.5 Material Removal Mechanism

Load per particle (F_a) is calculated using Eqs. (7)-(16) and is shown in Table 5. It is observed to lie in the range of 0.18 $\times$ 10^{-6} to 4.1 $\times$ 10^{-6} N during the polishing of BK7 optical glass for a range of parameters mentioned in Table 5. Yu et al. [49, 50] have also reported the load per particle of the order of micro-newton (10^{-6} N) measured using an Atomic Force Microscope (AFM). The load per particle tends to decrease with polishing time. It may be explained as: as the abrasive slurry is poured at a constant interval of time, the effective number of particles present at the interface increases with time, hence, the load per particle decreases.

According to Preston's equation [51]:

$$MRR = kpv \qquad (31)$$

Table 6 ANOVA results for friction coefficient

Source	DF	Seq SS	Adj SS	Adj MS	F	P
Regression	6	0.0863165	0.0863165	0.0143861	501.471	0.000000
Abrasive size	1	0.0151735	0.0023238	0.0023238	81.003	0.000002
Normal load	1	0.0013568	0.0001105	0.0001105	3.853	0.075446
Relative velocity	1	0.0682449	0.0009539	0.0009539	33.252	0.000125
Abrasive size*normal load	1	0.0000047	0.0000047	0.0000047	0.164	0.693145
Abrasive size*relative velocity	1	0.0015341	0.0015341	0.0015341	53.477	0.000015
Normal load*relative velocity	1	0.0000024	0.0000024	0.0000024	0.083	0.779198
Error	11	0.0003156	0.0003156	0.0000287		
Total	17	0.0866320				
Summary of model	$R^2 = 99.64\%$, R^2 (adj) = 99.44%, R^2 (pred) = 99.09%					

Table 7 ANOVA results for MRR

Source	DF	Seq SS	Adj SS	Adj MS	F	P
Regression	6	0.874681	0.874681	0.145780	64.1236	0.000000
Abrasive size	1	0.084828	0.001658	0.001658	0.7293	0.411326
Normal load	1	0.610741	0.050269	0.050269	22.1115	0.000648
Relative velocity	1	0.145886	0.000021	0.000021	0.0091	0.925808
Abrasive size*normal load	1	0.012208	0.012208	0.012208	5.3700	0.040769
Abrasive size*relative velocity	1	0.020919	0.020919	0.020919	9.2016	0.011380
Normal load*relative velocity	1	0.000098	0.000098	0.000098	0.0430	0.839505
Error	11	0.025008	0.025008	0.002273		
Total	17	0.899689				
Summary of model	$R^2 = 97.22\%$, R^2 (adj) = 95.70%, R^2 (pred) = 91.95%					

where k is Preston constant (m^2/N), p is applied load per unit area (N/m^2) and v is relative motion (m/s). Here, $p \times v$ is nothing but work done by applied load per unit area per unit time. For the present study, work done by the applied load per unit area per unit time is calculated as:

$$W = \frac{F_a N_s v}{A} \qquad (32)$$

where N_s and F_a are obtained from Eqs. (15) and (16) and are tabulated in Table 5. Hence, Preston's constant (k) is calculated as:

$$k = \frac{MRR}{W} \qquad (33)$$

The values of Preston's constant are observed to be in the range of 1.6196×10^{-13} to 3.81789×10^{-13} for BK7 glass polishing, which is quite similar to those obtained through experimental results (k_R: 2.1632×10^{-13} to 3.75145×10^{-13}

m^2/N), with an average error of 17.8%. Similar values of Preston's constant are reported by Suratwala et al. [52, 53].

Based on the values of load per particle, it may be concluded that during the polishing of BK7 optical glass material is removed from the workpiece surface using mechanical (plastic removal) as well as chemical actions, but as BK7 is chemically inert [23] and load per particle is close to critical load (5×10^{-5} N), reported by Suratwala et al. [26], mechanical actions are dominant over chemical actions. The values of friction coefficient (~ 0.1) also suggest that the workpiece and polisher are in solid–solid contact mode and hence, the material is removed mainly by mechanical forces [16].

Material removal mechanism is also demonstrated through observation of surface texture through CCI Optics (Coherence Correlation Interferometry-based non-contact optical profiler) of different polished samples. The samples are chosen considering the range of friction coefficient observed, shown in Fig. 8. It is observed that as the friction coefficient increases mechanism of material removal shifts from ductile to brittle.
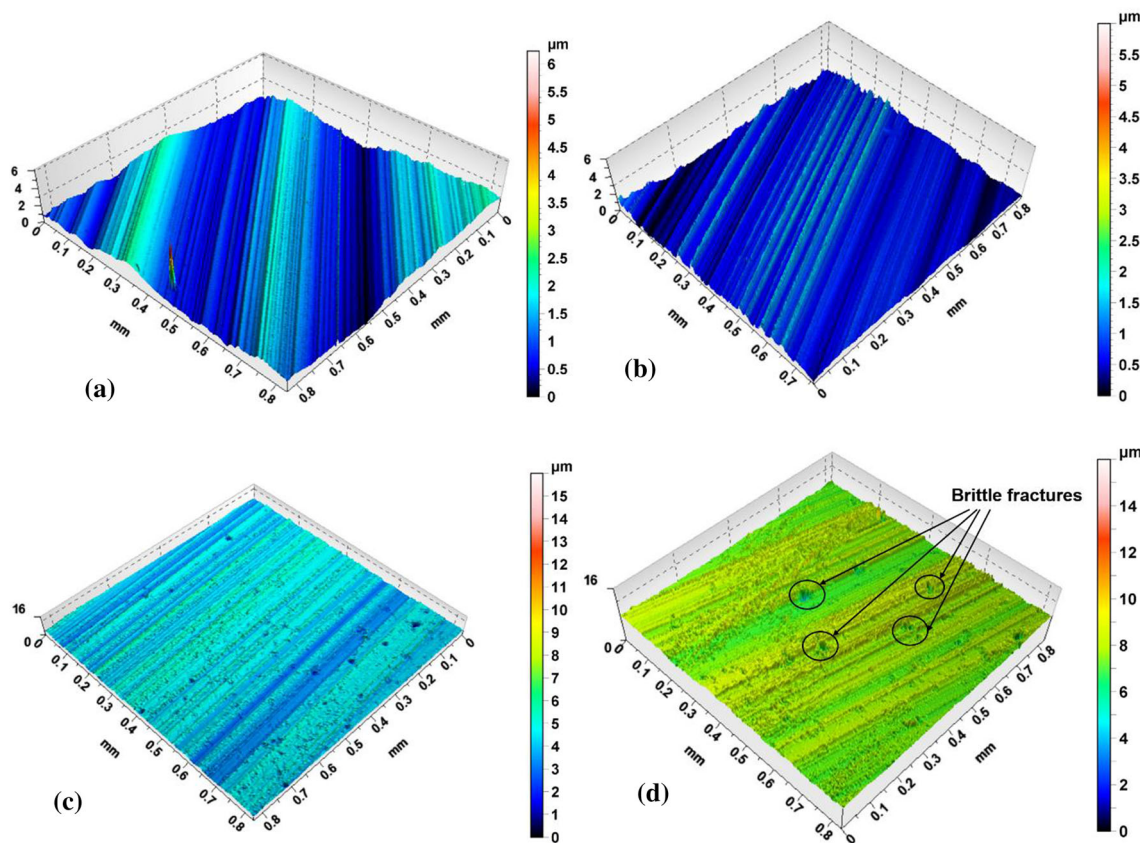
Fig. 8 Surface texture observed through CCI Optics, **a**: $\mu < 0.15$, material is removed through ductile material removal mechanism; **b**: $0.15 < \mu < 0.25$, material is mostly removed through ductile material removal mechanism, except in few zones; **c**: $0.25 < \mu < 0.30$, material is removed through ductile material removal mechanism, however, brittle fractures have initiated; and **d**: $\mu > 0.30$, along with ductile material removal, brittle fractures can be easily observed

5 Conclusions

In the present study, an empirical model was developed to predict the friction coefficient and material removal rate during the polishing of Bk7 optical glass considering the abrasive size, normal load, and relative velocity as governing input parameters. The developed models were validated through experimental study. From the study, the following observations could be drawn:

i.   The friction coefficient at the polishing interface is observed to be a function of abrasive size, normal load, and relative velocity. Following mathematical expression, based on the Sigmoidal curve, is obtained: $= 1 - \frac{0.274}{1 - 2.2e^{-\left(\frac{a^{1/3}L^{1/4}}{v}\right)^{0.112}}}$. Similarly, the material removal rate is observed to be a function of friction coefficient, normal load, and relative velocity. The following mathematical expression is obtained: $MRR = k_R \times p \times v$, where k_R is equal to $c_1\mu^\gamma$ (modified Preston's constant

based on experimental data), whose values lie in the range of 2.1632×10^{-13} to 3.75145×10^{-13} m²/N.

ii. The mathematical formulations for friction coefficient and MRR were validated by repeating three sets of experiments. The error between measured and calculated values is within 8% for friction coefficient and 12% for MRR. Further, Load per particle is modeled and its values are observed to lie in the range of 0.18×10^{-6} to 4.1×10^{-6} N during the polishing of BK7 optical glass.

iii. The separate Preston's constant (k) is determined based on the work done by the calculated active abrasive particles bearing the load, whose values are observed to lie in the range of 1.6196×10^{-13} to 3.81789×10^{-13} for BK7 glass polishing, which is quite similar to those obtained through experimental results (k_R: 2.1632×10^{-13} to 3.75145×10^{-13} m²/N). Hence, it may be stated that assumptions used for modeling load per particle are justified.

iv. Further, based on the values of load per particle, it may be concluded that during polishing of BK7 optical glass material is removed from the workpiece surface using

mechanical (plastic or ductile removal) as well as chemical actions, however, considering the chemical inertness of BK7 optical glass and value of load per particle close to critical load (5×10^{-5} N), mechanical actions are found to be dominant in material removal. The values of the friction coefficient (~ 0.1) also support this statement.

v. Material removal mechanism is also demonstrated through CCI images of surface texture observed for some of the glass samples. It is inferred that material removal shifts from ductile to brittle as the friction coefficient at the workpiece-polisher interface increases.

The CMP is a complex hybrid process where the process is mainly governed by chemical reactions and mechanical action. The present numerical study is a step forward in analyzing the CMP process for better control and accuracy to meet the dynamic demands of the industry. More chemical-specific material removal studies may be attempted by considering more input and response parameters along with surface morphology.

Authors' Contributions RKP contributed to conceptualization, resources, methodology, data curation, software, formal analysis, supervision, validation, investigation, writing—reviewing and editing, and project administration. MK contributed to data curation, formal analysis, methodology, software, visualization, and investigation. VK contributed to resources, visualization, supervision, validation, and project administration.

Availability of Data and Materials All data generated or analyzed during this study are included in this published article.

Declarations

Conflict of interest The authors declare that they have no known competing financial interests or personal relationships that could have appeared to influence the work reported in this paper. The authors declare that they have no conflict of interest.

Ethics Approval For this type of study formal consent is not required.

Consent to Participate Not applicable.

Consent to Publication Not applicable for this type of study.

Research Involving Human Participants and/or Animals Not applicable.

Informed Consent Not applicable.

References

1. Jain, V.K.; Balasubramaniam, R.; Mote, R.G.; Das, M.; Sharma, A.; Kumar, A.; Garg, V.; Kamaliya, B.: Micromachining: an overview (Part I) **3**, 142–158 (2020). https://doi.org/10.1177/2516598419895828

2. Yu, T.; Li, H.; Wang, W.: Experimental investigation on grinding characteristics of optical glass BK7: with special emphasis on the effects of machining parameters. Int. J. Adv. Manuf. Technol. **82**, 1405–1419 (2016). https://doi.org/10.1007/s00170-015-7495-2

3. Kumar, M.; Vaishya, R.O.; Oza, A.D.; Suri, N.M.: Experimental investigation of wire-electrochemical discharge machining (WECDM) performance characteristics for quartz material. SILICON **12**, 2211–2220 (2020). https://doi.org/10.1007/s12633-019-00309-z

4. Baisden, P.A.; Atherton, L.J.; Hawley, R.A.; Land, T.A.; Menapace, J.A.; Miller, P.E.; Runkel, M.J.; Spaeth, M.L.; Stolz, C.J.; Suratwala, T.I.; Wegner, P.J.; Wong, L.L.: Large optics for the national ignition facility. Fusion Sci. Technol. **69**, 295–351 (2016). Doi: https://doi.org/10.13182/FST15-143

5. Savio, G.; Pal, R.K.; Meneghello, R.; D'Angelo, L.; Concheri, G.: Shape and curvature error estimation in polished surfaces of ground glass molds. Optice. **56**, 024101–024101 (2017)

6. Meneghello, R.; Concheri, G.; Savio, G.; Comelli, D.: Surface and geometry error modeling in brittle mode grinding of ophthalmic lenses moulds. Int. J. Mach. Tools Manuf **46**, 1662–1670 (2006). https://doi.org/10.1016/j.ijmachtools.2005.08.016

7. Alam, Z.; Khan, D.A.; Jha, S.: A study on the effect of polishing fluid volume in ball end magnetorheological finishing process. Mater. Manuf. Process. **33**, 1197–1204 (2018). https://doi.org/10.1080/10426914.2017.1364760

8. Savio, G.; Meneghello, R.; Concheri, G.: A surface roughness predictive model in deterministic polishing of ground glass moulds. Int. J. Mach. Tools Manuf **49**, 1–7 (2009). https://doi.org/10.1016/j.ijmachtools.2008.09.001

9. Pal, R.K.; Garg, H.; Sarepaka, V.; Karar, V.: Experimental investigation of material removal and surface roughness during optical glass polishing. Mater Manuf. Process. **31**, 1613–1620 (2016)

10. Pal, R.K.; Garg, H.; Karar, V.: Material removal characteristics of full aperture optical polishing process. Mach. Sci. Technol. **21**, 493–525 (2017). https://doi.org/10.1080/10910344.2017.1336626

11. Wang, G.; Zhou, X.; Meng, G.; Yang, X.: Modeling surface roughness for polishing process based on abrasive cutting and probability theory. Mach. Sci. Technol. **22**, 86–98 (2018). https://doi.org/10.1080/10910344.2017.1336629

12. Cook, L.M.: Chemical processes in glass polishing. J. Non-Cryst. Solids **120**, 152–171 (1990). https://doi.org/10.1016/0022-3093(90)90200-6

13. Krishnan, M.; Nalaskowski, J.W.; Cook, L.M.: Chemical mechanical planarization: Slurry chemistry, materials, and mechanisms. Chem. Rev. **110**, 178–204 (2010). https://doi.org/10.1021/cr900170z

14. Wang, C.C.; Lin, S.C.; Hochen, H.: A material removal model for polishing glass-ceramic and aluminum magnesium storage disks. Int. J. Mach. Tools Manuf **42**, 979–984 (2002). https://doi.org/10.1016/S0890-6955(02)00004-4

15. Werrell, J.M.; Mandal, S.; Thomas, E.L.; Brousseau, E.B.; Lewis, R.; Borri, P.; Davies, P.R.; Williams, O.A.: Effect of slurry composition on the chemical mechanical polishing of thin diamond films. Sci. Technol. Adv. Mater. **18**, 654–663 (2017)

16. Evans, C.J.; Paul, E.; Dornfield, D.; Lucca, D.A.; Byrne, G.; Tricard, M.; Klocke, F.; Dambon, O.; Mullany, B.A.: Material removal mechanisms in lapping and polishing. CIRP Ann. Manuf. Technol. **52**, 611–633 (2003). https://doi.org/10.1016/S0007-8506(07)60207-8

17. Lai, J.Y.: Mechanics, mechanisms, and modeling of the chemical mechanical polishing process, in: Department of Mechanical Engineering, Massachusetts Institute of Technology, pp. 308 (2001)

18. Pal, R.K.; Garg, H.; Karar, V.: Full aperture optical polishing process: Overview and challenges. Lecture Notes in Mechanical Engineering. 461–470 (2016). Doi: https://doi.org/10.1007/978-81-322-2740-3_45

19. Suratwala, T.I.; Feit, M.D.; Steele, W.A.: Toward deterministic material removal and surface figure during fused silica pad polishing. J. Am. Ceram. Soc. **93**, 1326–1340 (2010). https://doi.org/10.1111/j.1551-2916.2010.03607.x

20. Belkhir, N.; Bouzid, D.; Herold, V.: Determination of the friction coefficient during glass polishing. Tribol. Lett. **33**, 55–61 (2009). https://doi.org/10.1007/s11249-008-9391-5

21. Belkhir, N.; Aliouane, T.; Bouzid, D.: Correlation between contact surface and friction during the optical glass polishing. Appl. Surf. Sci. **288**, 208–214 (2014). https://doi.org/10.1016/j.apsusc.2013.10.008

22. Kelm, A.; Boerret, R.; Sinzinger, S.: Improving the polishing accuracy by determining the variance of the friction coefficient. J. Eur. Opt. Soc. **7**, (2012). Doi: https://doi.org/10.2971/jeos.2012.12049

23. Yu, J.; Yuan, W.; Hu, H.; Zang, H.; Cai, Y.; Ji, F.: Nanoscale friction and wear of phosphate laser glass and BK7 glass against single CeO2 particle by AFM. J. Am. Ceram. Soc. **98**, 1111–1120 (2015). https://doi.org/10.1111/jace.13356

24. Suratwala, T.; Steele, W.; Feit, M.; Shen, N.; Dylla-Spears, R.; Wong, L.; Miller, P.; Desjardin, R.; Elhadj, S.; Pharr, G.: Mechanism and simulation of removal rate and surface roughness during optical polishing of glasses. J. Am. Ceram. Soc. **99**, 1974–1984 (2016). https://doi.org/10.1111/jace.14220

25. Almeida, R.; Börret, R.; Rimkus, W.; Harrison, D.K.; DeSilva, A.K.M.: Material removal simulation for steel mould polishing. Prod. Manuf. Res. **5**, 235–249 (2017). https://doi.org/10.1080/21693277.2017.1374889

26. Suratwala, T.; Feit, M.; Steele, W.; Wong, L.; Shen, N.; Dylla-Spears, R., et al.: Microscopic removal function and the relationship between slurry particle size distribution and workpiece roughness during pad polishing. J. Am. Ceram. Soc. **97**, 81–91 (2014)

27. Deng, C.; Jiang, L.; Qin, N.; Qian, L.: Effects of pH and H_2O_2 on the chemical mechanical polishing of titanium alloys. J. Mater. Process. Technol. **295** (2021). Doi: https://doi.org/10.1016/j.jmatprotec.2021.117204

28. Deng, C., Jiang, L., & Qian, L.: High-efficiency chemical mechanical polishing of Ti-6Al-4V alloy via the synergistic action of H_2O_2 and K+ under alkaline conditions. ECS J. Solid State Sci. Technol. **11**, 024005 (2022)

29. Liang, H.; Kaufman, F.; Sevilla, R.; Anjur, S.: Wear phenomena in chemical mechanical polishing. Wear **211**, 271–279 (1997). https://doi.org/10.1016/S0043-1648(97)00124-5

30. Luo, Q.; Ramarajan, S.; Babu, S.V.: Modification of the Preston equation for the chemical-mechanical polishing of copper. Thin Solid Films **335**, 160–167 (1998). https://doi.org/10.1016/S0040-6090(98)00896-7

31. Srinivasa-Murthy, C.; Wang, D.; Beaudoin, S.P.; Bibby, T.; Holland, K.; Cale, T.S.: Stress distribution in chemical mechanical polishing. Thin Solid Films **308–309**, 533–537 (1997). https://doi.org/10.1016/S0040-6090(97)00433-1

32. Lee, H.; Kim, H.; Jeong, H.: Approaches to sustainability in chemical mechanical polishing (CMP): a review. Int. J. Precision Eng. Manuf. Green Technol. **9**, 349–367 (2021). https://doi.org/10.1007/s40684-021-00406-8

33. Seo, J.: A review on chemical and mechanical phenomena at the wafer interface during chemical mechanical planarization. J. Mater. Res. **36**, 235–257 (2021). https://doi.org/10.1557/s43578-020-00060-x

34. Terrell, E.J.; Higgs, C.F.: Hydrodynamics of slurry flow in chemical mechanical polishing: a review. J. Electrochem. Soc. **153**, K15 (2006). https://doi.org/10.1149/1.2188329

35. Pal, R. K., Kumar, M., Karar, V.: Experimental investigation of polishing process for Schott BK-7 optical glass. In: Materials Today: Proceedings, **57**, 734–738 (2022). Doi: https://doi.org/10.1016/j.matpr.2022.02.218

36. Kumar, S.; Singh, A.K.: Magnetorheological nanofinishing of BK7 glass for lens manufacturing. Mater. Manuf. Processes **33**, 1188–1196 (2018). https://doi.org/10.1080/10426914.2017.1364759

37. Sharma, R.; Mishra, V.; Khatri, N.; Garg, H.; Karar, V.: A hybrid fabrication approach and profile error compensation for silicon aspheric optics. Proc Inst Mech Eng Part B J Eng Manuf. **233**, 1600–1607 (2019). https://doi.org/10.1177/0954405417733018

38. Tsegaw, A.A.; Shiou, F.J.; Lin, S.P.: Ultra-precision polishing of N-Bk7 using an innovative self-propelled abrasive fluid multi-jet polishing tool. Mach. Sci. Technol. **19**, 262–285 (2015). https://doi.org/10.1080/10910344.2015.1018532

39. Moses, E.I.: Advances in inertial confinement fusion at the National Ignition Facility (NIF). Fusion Eng. Des. **85**, 983–986 (2010). https://doi.org/10.1016/j.fusengdes.2009.11.006

40. Limbach, R.; Winterstein-Beckmann, A.; Dellith, J.; Möncke, D.; Wondraczek, L.: Plasticity, crack initiation and defect resistance in alkali-borosilicate glasses: From normal to anomalous behavior. J. Non-Cryst. Solids **417–418**, 15–27 (2015). https://doi.org/10.1016/j.jnoncrysol.2015.02.019

41. Preedy, E.; Perni, S.; Nipiĉ, D.; Bohinc, K.; Prokopovich, P.: Surface roughness mediated adhesion forces between borosilicate glass and gram-positive bacteria. Langmuir **30**, 9466–9476 (2014). https://doi.org/10.1021/la501711t

42. Jain, V.K.; Sidpara, A.; Sankar, M.R.; Das, M.: Nano-finishing techniques: A review. Proc. Inst. Mech. Eng. C J. Mech. Eng. Sci. **226**, 327–346 (2012). https://doi.org/10.1177/0954406211426948

43. U.P. Incorporated, LP UNALON - Precision polishing material engineered to deliver superior flatness & higher removal rates. In: U.P. Incorporated (Ed.) Innovative Polishing Material, Universal Photonics Incorporated, USA, (2015

44. Greenwood, J.A.; Williamson, J.B.P.: Contact of nominally flat surfaces. Proc. R. Soc. Lond. A **295**, 300–319 (1966)

45. Popov, V.: Rigorous Treatment of Contact Problems—Hertzian Contact, In: Contact Mechanics and Friction, Springer, Heidelberg, 2010, pp. 55–70.Sdas

46. Meyer, K.; Polzer, G.; Meissner, F.: Grundlagen zu Reibung und Verschleiß. VEB Deutscher Verlag für Grundstoffindustrie Leipzig, Leipzig 1983, 2., durchgesehene u. erweiterte Auflage mit 340 S., 156 Bildern und 40 Tabellen, Preis: M 35,—, Cryst Res Technol, 19 (1984) K35-K35

47. Johnson, K.L.: One hundred years of hertz contact. Proc. Inst. Mech. Eng. **196**, 363–378 (1982). https://doi.org/10.1243/PIME_PROC_1982_196_039_02

48. Tesar, A.A.; Fuchs, B.A.: Removal rates of fused silica with cerium oxide/pitch polishing. In: Doherty, V.J. (Ed.) Advanced Optical Manufacturing and Testing II, pp. 80–90. SPIE (1992)

49. Yu, J.; He, H.; Zhang, Y.; Hu, H.: Nanoscale mechanochemical wear of phosphate laser glass against a CeO_2 particle in humid air. Appl. Surf. Sci. **392**, 523–530 (2017). https://doi.org/10.1016/j.apsusc.2016.09.061

50. Yu, J.; Hu, H.; Jia, F.; Yuan, W. ,Zang, H.; Cai, Y.; Ji F.: Quantitative investigation on single-asperity friction and wear of phosphate laser glass against aspherical AFM diamond tip. Tribol. Int., pp. 43–52. (2015)

51. Preston, F.W.: The theory and design of plate glass polishing machine. J. Soc. Glas. Technol. **11**, 214–256 (1927)

52. Suratwala, T.; Steele, W.A.; Feit, M.D. et al.: Mechanisms and control of surface figure & roughness during pad polishing. In: Optical Fabrication and Testing, OSA, Kohala Coast, Hawaii, USA (2014)

53. Suratwala, T.; Steele, R.; Feit, M., et al.: Convergent polishing: a simple, rapid, full aperture polishing process of high quality optical flats & spheres. J. Vis. Exp. **94**, 1–10 (2014). https://doi.org/10.3791/51965